

Remote leveling of tide gauges using GNSS reflectometry: case study at Spring Bay, Australia

Alvaro Santamaría-Gómez^{1,2} · Christopher Watson²

Received: 6 October 2015 / Accepted: 7 April 2016 / Published online: 18 April 2016
© Springer-Verlag Berlin Heidelberg 2016

Abstract We further developed a new approach using GNSS reflectometry to determine the leveling connection between a tide gauge and a GNSS antenna. This approach includes the optimization of the unknown receiver bandwidth and the estimation of frequency changes in the signal-to-noise ratio (SNR) oscillation through an extended Kalman filter/smoothing algorithm. We also corrected the geometric bending of the GNSS signals due to tropospheric refraction using local meteorological observations. Using 3 weeks of SNR data in Spring Bay, Australia, from a GNSS antenna placed sideways (i.e., ground plane orientated vertically and directed in azimuth toward the sea surface) to improve the SNR interference near the horizon, we obtained mean leveling differences of approximately 5 mm, with an RMS of approximately 3 cm level with respect to the nominal leveling from classical surveying techniques. SNR data from three different receiver manufacturers, coupled to the same antenna, provided similar leveling results. With a second antenna in the usual upright configuration, we obtained mean leveling differences of 1–2 cm and a RMS of about 10 cm. In the upright configuration, the leveling differences may include errors in the GNSS antenna phase center calibration, which are avoided in our technique but not in the classical surveying techniques. These results demonstrate the usefulness of the reflectometry technique to obtain precisely and remotely

the leveling between a GNSS antenna and a tide gauge. In addition, this technique can be applied continuously, providing an independent and economical means to monitor the stability of the tide gauge zero.

Keywords Reflectometry · GNSS · SNR · Tide gauge · Leveling · Atmospheric refraction

Introduction

We develop the GNSS reflectometry tie technique for leveling co-located GNSS and tide gauge (TG) stations suggested by Santamaría-Gómez et al. (2015). This technique allows one to estimate the vertical distance between the TG zero and the phase center of a co-located GNSS antenna using reflections of GNSS signals from the sea surface together with the TG observations of the sea-surface height (SSH). The radio signals reflected from the sea surface and reaching the GNSS antenna are delayed with respect to the direct signal and cause measurable interference in the form of an oscillation of the recorded signal-to-noise ratio (SNR). By analyzing the rate of change of the SNR oscillation, we can estimate the vertical distance from the sea surface to the GNSS antenna. The GNSS reflectometry technique using SNR data has been used in the past to obtain SSH which used TG observations as ground truth (Anderson 2000; Benton and Mitchell 2011; Larson et al. 2013a, b; Löfgren et al. 2014). Here, the TG observations are used to remove the time-variable SSH variations, e.g., the tide, and translate the measured distance from the sea surface to the TG zero, providing the desired leveling distance.

This new technique provides several advantages compared to the in situ leveling from classical surveying

✉ Alvaro Santamaría-Gómez
alvaro.santamaria@univ-lr.fr

¹ LIENSs, Université de La Rochelle/CNRS, La Rochelle, France

² Surveying and Spatial Sciences, School of Land and Food, University of Tasmania, Private Bag 76, Hobart, Tasmania 7001, Australia

techniques that is used, or could be used, at many TGs. It can be performed remotely, thus minimizing the need for dedicated economic resources. It allows the leveling of GNSS stations that would otherwise be difficult to access or level, as in rooftop installations. It allows the leveling to be performed continuously or backward in time as long as GNSS and TG observations are coincident. And finally, it avoids errors in the calibration of the GNSS and TG references while allowing for the monitoring of their relative stability. Despite these clear advantages, this technique requires further developments to improve its accuracy in comparison with what is obtained with classical leveling (Santamaría-Gómez et al. 2015). Specifically, Santamaría-Gómez et al. (2015) found an elevation-dependent leveling bias of the order of about 10 cm when using satellite observations below 12° elevation. A plausible origin for the elevation-dependent error is the geometric bending of the GNSS signals due to tropospheric refraction (Roussel et al. 2014). The elevation-dependent error is the most limiting factor for the broad application of this technique given that SNR series at very low observations are usually required for the conventional application of this technique.

Santamaría-Gómez et al. (2015) also found that in two out of eight stations leveled (Burnie and Spring Bay, Australia), the technique provided a systematic leveling bias of about 10–12 cm. Both stations are equipped with the same GNSS and TG instruments. A follow-on experiment was conducted in Spring Bay with the objective of developing the technique and improving the results obtained thus far. Specifically, we implemented a dedicated field experiment to address two questions: Do different receivers and signals provide different leveling results at the same site that could explain the leveling bias? And, is the elevation-dependent leveling bias explained from the geometric bending produced by tropospheric refraction?

The Spring Bay experiment

From January 7–30, 2015, a field experiment was carried out at the TG station at Spring Bay, Tasmania, Australia. This station forms part of the Australian Baseline Sea Level Monitoring Project (ABSLMP)¹ operated by the Australian Bureau of Meteorology. It is an easy access and well-instrumented site offering a wide horizon of approximately 170° of sea-surface reflections (Fig. 1). It has an Aquatrak acoustic TG sensor, a Vegapuls radar TG sensor, a permanent GPS station (SPBY) and a meteorological station recording barometric pressure and air/water temperature (Fig. 2). The permanent GPS station is equipped with a geodetic Leica AT504 GG antenna with a SCIS

¹ <http://www.bom.gov.au/oceanography/projects/abslmp/data/index.shtml> last accessed January 2016.

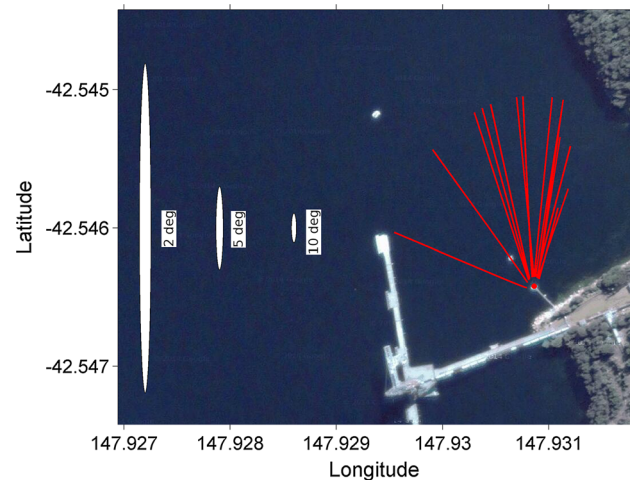


Fig. 1 Aerial view of the Spring Bay site (solid red circle) with the location of the processed satellite ground tracks between 2° and 40° elevation (red lines). Note that only satellites transmitting L2C are shown. The sizes of the first Fresnel zone at different satellite elevation angles are also shown (white areas). A mean reflector height of 3.94 m and the L1 carrier were used to compute the satellite ground tracks and the first Fresnel zones

radome and a geodetic Leica GRX1200 GG receiver recording L1 and L2P data at 1 Hz. No L2C observables are available from this station.

During the experiment, three GNSS receivers, a Leica GRX1200, a Trimble NetR9 and a Septentrio PolaRxS Pro, were recording GPS L1 and L2 signals at 1 Hz from a common shared antenna of the same type as for the permanent station, a Leica AT504 GG. Both L2P and L2C codes were tracked. The antenna was placed sideways between 3 and 5 m above the sea surface, with the ground plane vertical, and directed in azimuth to face the sea surface using the same monument as the upright permanent antenna (Fig. 2). Given the fixed antenna gain pattern, orientating the antenna sideways changes the ratio of the direct to reflected signal strengths compared to the upright case, thus maximizing the interference of the reflected signals and providing clearer SNR oscillations that persist to higher elevation angles (Fig. 3). The longer record of the SNR oscillation increases the frequency resolution and improves the formal precision of the estimated frequency of the oscillation. A better frequency resolution may also help to discriminate non-stationary features in the spectral domain such as spurious frequency drifts from unmodeled tropospheric refraction, near-field multipath, sea-surface flatness, etc.

We noticed different tracking performance of the three receivers sharing the antenna during the experiment, with gaps at different epochs. The Septentrio receiver gathered longer and more continuous observations, probably due to its settings allowing the tracking of noisier GPS signals



Fig. 2 Northward view of the Spring Bay site, Australia. The labels indicate the location of each instrument. The air gap distance from the acoustic TG to the mean sea-level surface during the experiment is approximately 3.6 m

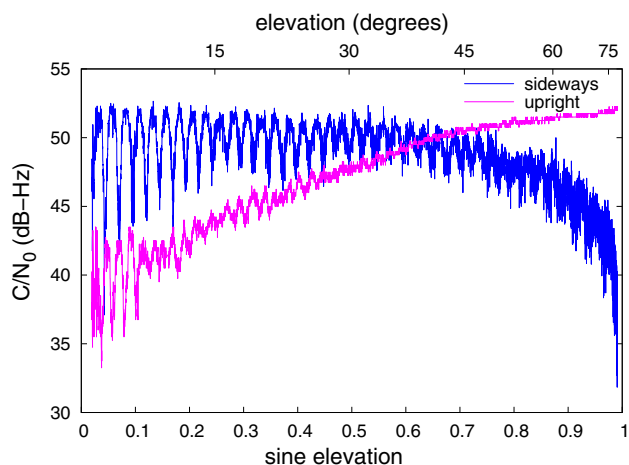


Fig. 3 Carrier-to-noise density ratio (C/N_0) observations in dB-Hz from the sideways (blue) and upright (pink) antennas for the same transmitted L1 signal and same receiver model. These observations are equivalent to SNR in dB assuming a noise bandwidth of 1 Hz

compared to the Leica and Trimble receivers. Nevertheless, the shape of the carrier-to-noise density ratio (C/N_0) oscillation in L1 and L2C was consistent among all the receivers. In general, the C/N_0 oscillations in L2C were smaller in magnitude and diminished with elevation faster

than the SNR oscillations in L1. The tracking in L2P was more receiver-dependent, with the Trimble receiver showing very low C/N_0 with frequent gaps, especially at high elevation. This could be due to the receiver-specific tracking algorithms, the performance of the antenna splitter, or the shared antenna being a Leica and being powered by the Leica receiver.

The reference marks of both TGs and both GNSS antennas were leveled using classical in situ surveying techniques, confirming previous leveling results available at this site with a difference of less than 1 mm. The calibrated location of the TG zero with respect to the reference mark and the time series of the measured air gap distance from each TG zero to the sea surface were then used to close the leveling loop. The leveling loop includes the air gap from the acoustic TG zero to the sea surface, the air gap between the sea surface to the radar TG zero, and the leveling between both TG zeroes plus their calibration. The loop closed with a mean error of -6 mm, fluctuating in time between 4.7 and -19.3 mm (95 % interval) with a standard deviation of 8 mm. The consistency of the leveling results excludes a leveling error as the main contributor to the mean closure error. Therefore, the closure error probably accounts for a time-dependent measurement bias in one of the TG sensors or in both. While the acoustic sensor automatically applies corrections to the temperature-driven changes of the speed of sound, a small fraction of the variation of the closure error may originate from uncorrected temperature gradients (Hunter 2003) and/or current-driven Bernoulli effects (Shih and Rogers 1981) inside the acoustic sounding tube. However, it was not possible to allocate a time-variable measurement bias to any of the TG sensors without additional independent measurements of the SSH. On the other hand, it is more likely that any time constant closure error originates from the zero calibration of the radar TG, which was obtained from the manufacturer, in contrast to the zero calibration of the acoustic TG which was determined in a laboratory setting by the station manager (Bureau of Meteorology, personal communication). Therefore, in what follows, we used SSH measured by the acoustic sensor alone assuming it is free of any measurement bias. SSH uncertainty from the acoustic sensor places the upper limit of the contribution of the TG calibration to the leveling estimates to within 8 mm. This error is small enough to rule out the calibration of the TG zero as the origin of the about 12-cm leveling bias found at this station by Santamaría-Gómez et al. (2015), leaving the processing of the SNR data as the likely origin of the reported leveling bias. In the next section, we refine the SNR signal processing approach to address this problem.

Processing the SNR signal

The GNSS receiver C/N_0 measurements for each ascending/descending satellite arc are converted to SNR data, detrended and translated in height to the TG zero by removing the observed SSH. Then, the vertical distance between the GNSS antenna phase center and the TG zero is linearly given by the frequency of the SNR oscillation and

$$h = \frac{\lambda}{2}f \quad (1)$$

where f is the estimated frequency of the SNR oscillation in cycles per sine of elevation and λ is the GNSS transmitted signal wavelength. Further details are provided in earlier studies using SNR measurements where the dynamic SSH needed to be accounted for (Larson et al. 2013b; Löfgren et al. 2014). The next sections describe the developments of the SNR signal processing.

Converting the SNR signal

Before processing the SNR signal, the C/N_0 measurements in dB-Hz are usually converted into SNR values following:

$$\text{SNR} = \frac{C}{N_0B} \quad (2)$$

where B is the noise bandwidth (in Hz) set in the receiver. We assume the reported S1/S2 values in the RINEX files are C/N_0 measurements. Depending on the receiver manufacturer, the noise bandwidth is usually not reported in the receiver settings or specifications. Fortunately, when using SNR measurements in logarithmic scale, the receiver's noise bandwidth acts as a scaling factor, and therefore, it has no effect on the estimated frequency of the SNR oscillation. Some authors choose to use SNR measurements in logarithmic scale assuming a noise bandwidth of 1 Hz (Larson et al. 2013a; Löfgren et al. 2014; Santamaría-Gómez et al. 2015). The caveat of this approach is that the SNR oscillation in logarithmic scale does not resemble a perfect sinusoidal oscillation and exhibits deep valleys and flat crests (Fig. 3). A transformation of the SNR measurements into linear scale (watts per watt or volts per volt), by taking the exponential of (2), also transforms the shape of the SNR data into a more sinusoid-like oscillation (Larson and Nievinski 2013; Nievinski and Larson 2014). However, when transforming from logarithmic to linear scale, the value of the noise bandwidth in (2) becomes critical as different bandwidth values yield different shapes of the resulting SNR oscillation, especially at low elevation angles where the amplitude of the SNR oscillation is larger. Depending on the noise bandwidth chosen, the SNR values at low elevation are distributed differently between the valleys/

crests of the oscillation; the lower the bandwidth value, the sharper the valleys and vice versa. The change in the shape of the SNR oscillation at low elevation as a function of the noise bandwidth may affect the sinusoidal fitting and the estimation of the frequency of the SNR oscillation, i.e., the distance to the reflecting surface.

The bandwidth values set in the receivers used here were unknown. Therefore, we developed an approach to optimize the bandwidth value for each receiver from the converted SNR data themselves. The optimization was based on the expected sinusoidal shape of the converted SNR. This was done by maximizing the explained variance of a fitted sinusoidal to the SNR data. SNR series with at least 3 SNR cycles below 7° were chosen to optimize the receiver bandwidth value between 2 and 50 Hz. At higher elevation, the changes in the sinusoidal shape of the oscillation by changing the bandwidth were more difficult to assess. Although the noise bandwidth set in the receiver is satellite-independent, the dispersion of the optimized bandwidth values varied for each GPS satellite and was not related to the satellite block. While some satellites had a narrow histogram of optimized bandwidth values with a standard deviation of 2–3 Hz, others provided scattered values and were not used to estimate the receiver bandwidth. The spread of bandwidth values for some satellites is probably caused by near-field multipath or by the different azimuthal obstructions of the signals at low elevation and the very repetitive ground track of the satellites within a month of observations. The average of the estimated bandwidth values for both L1 and L2 carriers were 7, 15 and 12 Hz, respectively, for the Leica, Trimble and Septentrio receivers, with uncertainties of less than 1 Hz. These values were then used to convert the S1/S2 (C/N_0) values reported in the RINEX files into linear SNR observables and then used to fit the frequency of the oscillation to determine the leveling.

Filtering the SNR signal

In Santamaría-Gómez et al. (2015), different leveling results were obtained using the L1 and L2(P) signals. In this experiment, we additionally used SNR observations from the L2(C) signal. In order to compare the performance of the GPS L1(C/A), L2(P) and L2(C) signals, only satellites transmitting the three codes were retained for further analysis. At the time of this experiment, this selection represents 15 satellites, about half the GPS constellation. To isolate the SNR series where the sea surface is the main reflector, we applied the stacked spectra approach described in Santamaría-Gómez et al. (2015), with the difference that we initially excluded satellite arcs not traversing the usable half-horizon of the antenna oriented sideways.

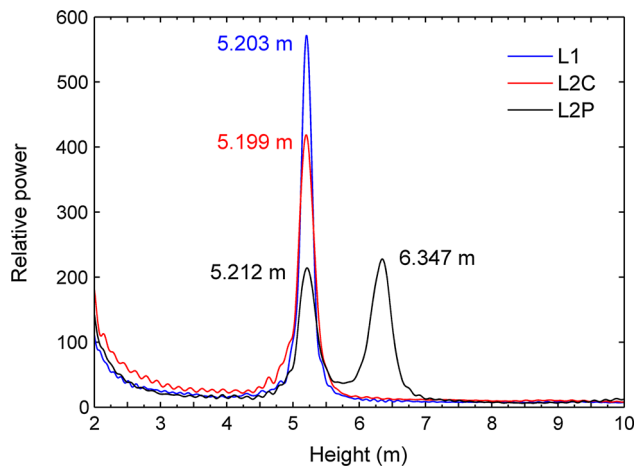


Fig. 4 Stacked Lomb–Scargle periodograms of the L1 (blue), L2(C) (red) and L2(P) (black) SNR series from the Septentrio receiver and the sideways antenna. Frequencies were transformed into heights at the corresponding L1 and L2 carrier wavelengths. The numbers indicate the height of the maximum power

Figure 4 shows the stacked Lomb–Scargle periodograms (Scargle 1982) from the three observed signals from the sideways antenna and the Septentrio receiver. The stacked periodograms compile data from the whole experiment duration and include about 330 satellite arcs. The stacked periodograms for the other receivers connected to the sideways antenna are similar and are not shown. The three signals are sensitive to the sea-surface reflections and provide a good a priori value of the vertical distance between the sideways antenna and the TG zero. However, a secondary artificial peak is also visible in the L2(P) periodogram (Fig. 4). The separation of this secondary peak for L2(P) does not exactly match with the location of a possible interference of the L1 carrier onto the SNR signal of the L2 carrier, which would be located at $\frac{\lambda_2}{\lambda_1} \simeq 1.283$ times the peak of the L2 carrier, where λ is the wavelength of the L1 and L2 carriers, respectively. In addition, this secondary peak is not visible in the stacked periodogram of the L2(P) signal from the upright antenna ruling out the L1 interference and the semi-codeless tracking of L2 as the plausible explanations. The origin of the secondary artificial peak in the L2(P) periodograms is elusive, but its location with respect to the main peak produced by the sea-surface reflections is consistent in all SNR series and for all receivers connected to the sideways antenna. This allows us to filter out this secondary SNR oscillation from the L2(P) SNR series by applying a band-pass filter. The band-pass filter was also used to remove very low SNR frequency variations located at least four times lower than the main frequency of interest provided by the stacked periodograms (Fig. 4). These long-period

variations of the SNR signal are due to the elevation-dependent antenna gain pattern (Fig. 3).

Estimating frequency changes in the SNR signal

Santamaría-Gómez et al. (2015) assumed the frequency of the SNR oscillation was constant once the inverse Doppler-like effect of the SSH change was corrected for using the TG measurements. Note that Eq. (5) in Santamaría-Gómez et al. (2015) for the inverse Doppler-like correction should read

$$\sin(e_i^k)' = \sin(e_i^k) \left(1 - \frac{\delta v_i^k}{v_i} \right) \tag{3}$$

$$\delta v_i^k = \frac{2}{\lambda} \delta h_i^k$$

where $\sin(e_i^k)'$ is the value of the independent variable, sine of elevation, after correction for the inverse Doppler-like effect; v_i is the instantaneous frequency at the beginning of the SNR series; δv_i^k is the frequency change from the beginning of the SNR series obtained from the observed SSH change with $\sin(e)$, δh_i^k ; λ represents the wavelength of the transmitted GPS signal. The frequency of the SNR oscillation is given in units of cycles per sine of elevation. Subscripts i refer to each SNR series, and superscripts k denote each individual SNR measurement in the series.

After correcting the SNR series for SSH changes, Santamaría-Gómez et al. (2015) estimated a constant frequency of the SNR oscillation while allowing the amplitude to vary through a Kalman filter. However, their results revealed a consistent elevation-dependent leveling bias in low-elevation SNR data. Here, we applied the same approach to remove the SSH changes and then we used a different approach based on a continuous epoch-wise estimation of the SNR frequency by means of a second-order extended Kalman filter/smoothers (EKF; Jazwinski (1966). The EKF is the evolution of the traditional Kalman filter dealing with nonlinear dynamical systems.

The initial amplitude and phase of the SNR oscillation in the EKF were obtained from an a priori sinusoid fit to the first four complete cycles of each SNR series, where the frequency was obtained from the a priori leveling value determined from the stacked periodograms (Fig. 4). The measurement noise variance in the EKF was obtained from the residuals of the sinusoidal fit. The phase of the estimated SNR oscillation was set as a constant, and we allowed the EKF to estimate variations in the amplitude and frequency of the SNR oscillation. The process noise variances for amplitude and frequency were tuned from synthetic data mimicking the SNR oscillation with different grades of amplitude and frequency variation. We retained estimated frequency values for which the estimated amplitude of the oscillation was twice the root mean square of the residual SNR signal after the EKF fit. For

most of the SNR series, this threshold allowed us to estimate frequency changes up to 40° elevation. Figure 5 shows an example of detrended SNR series (top panel in blue) and the estimated EKF oscillation model with the elevation-variable amplitude and frequency estimates (top panel in red, middle and bottom panels).

The geometric bending of the radio waves caused by the atmospheric refraction is one of the possible origins of the leveling bias at low elevation angles (Anderson 2000). The bending of the GNSS radio signals as they approach the earth's surface causes the actual incidence angle of the signals to differ with respect to the nominal satellite elevation at the GNSS antenna. This elevation-dependent elevation angle error affects the sampling of the SNR signal and mimics a drift in the frequency of the observed oscillation. This spurious Doppler-like effect can be removed if one knows the bending of the GNSS radio signals at the sea surface. Therefore, in a second processing of the SNR series, we applied the same strategy but, before running the EKF, the elevation angles [sine(e)] in the SNR series were corrected for the bending effect of the tropospheric refraction. The bending effect was estimated using atmospheric pressure and temperature recorded at the TG following (Bennett 1982):

$$\delta e = \frac{510}{5T + 492} \frac{P}{1010.16} \cot\left(e + \frac{7.31}{e + 4.4}\right) \quad (4)$$

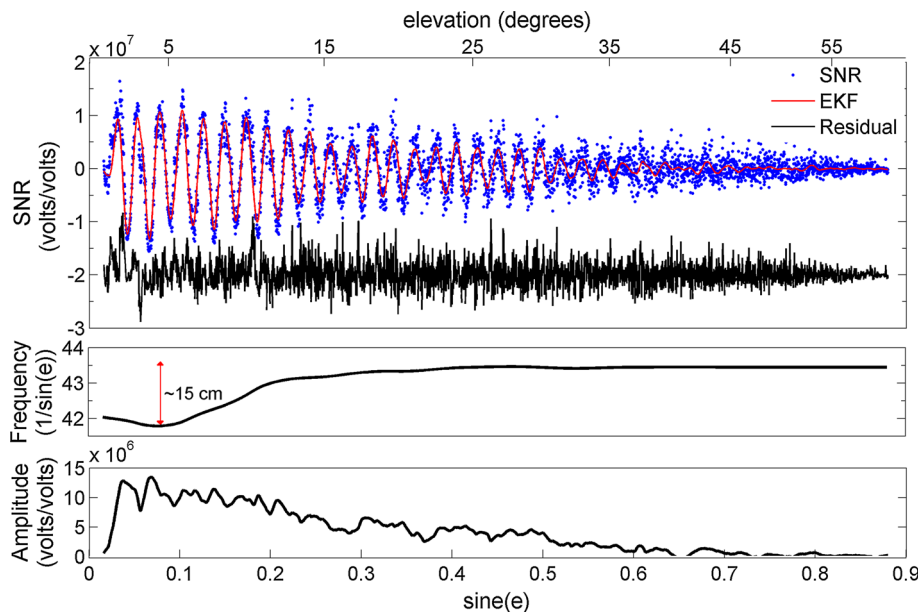
where e and δe is the elevation angle and the elevation angle change in radians, T is temperature in degrees C, and P is pressure in mb. The hourly tide gauge and meteorological data were obtained from the ABSLMP¹.

Results and discussion

A clear systematic elevation-dependent frequency variation, equivalent to up to about 15 cm in estimated height change, is shown in the example of Fig. 5. We applied the described approach to all recorded SNR series from different satellites, signals and receivers. Figure 6 shows the elevation-dependent leveling differences with respect to the nominal leveling value for each receiver and signal without applying (top) and after applying the bending correction of the elevation angles (bottom). Below 5° and above 25° elevation, all receivers show consistent results, but there is a separation of the leveling results by signal, with the L2(P) showing less leveling bias at low elevation in agreement with former results (Santamaría-Gómez et al. 2015). We also notice that the bending correction does not have the same impact in all the signals at low elevation. For instance, the leveling results in L2(P) below 5° elevation were degraded after applying the correction. This indicates that additional systematic errors also exist that may be signal-dependent. The secondary peak found in the L2(P) SNR spectra also supports this hypothesis.

Between 5° and 25° elevation, all signals and receivers show a consistent elevation-dependent leveling error below about 12° elevation (Fig. 6 top) reproducing the findings in Santamaría-Gómez et al. (2015). This elevation-dependent leveling bias is mostly reduced when applying the bending corrections (Fig. 6 bottom). Similar leveling results were obtained after applying the bending correction using (4) and temperature and pressure data extracted from the European Medium Range Weather Forecast ERA-Interim

Fig. 5 Example of elevation-dependent estimates of amplitude and frequency variations in a converted and band-pass-filtered L1 SNR series. *Top* observed SNR series (blue dots), estimated SNR model from the extended Kalman filter (red) and residuals (black). The filter residuals are presented with a 2 volts/volts offset for clarity reasons. *Middle* Elevation-dependent frequency estimates. A unit change in frequency roughly equals 10 cm height change. The red vertical arrow indicates the maximum apparent height change following (1). *Bottom* Elevation-dependent amplitude estimates



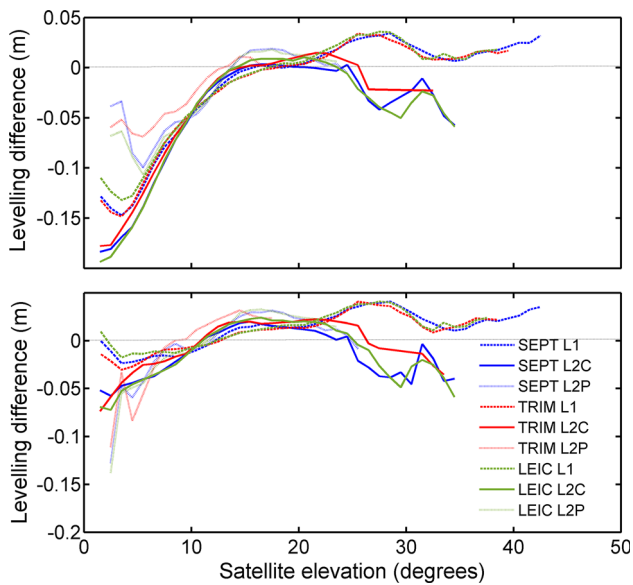


Fig. 6 Moving average of the leveling differences with respect to the nominal leveling value as a function of elevation angle by receiver and GPS signal (*top*) and after correcting for the bending effect (*bottom*). Differences are estimated leveling minus nominal leveling

(Dee et al. 2011) reanalysis, using a spatial resolution of 0.125° and a temporal resolution of 6 h. Therefore, the meteorological models may allow correcting for the bending effect easily at any location.

Table 1 shows the mean and standard deviation of the leveling differences with respect to the nominal leveling values for the different signals using SNR data from the Leica receiver above an elevation cutoff of 0° , 5° and 12° , respectively. Mean leveling differences between 2 to 7 mm were obtained above 5° elevation. Results for the Trimble and Septentrio receivers are similar to those for the Leica within this range. Some residual elevation-dependent error remains in the leveling differences after the bending correction is applied (Fig. 6) with a positive leveling bias between 1 and 2 cm above 12° elevation. We assume that

Table 1 Mean and standard deviation (mm) of the leveling differences for each antenna with respect to the nominal leveling value by GPS signal and elevation cutoff using the Leica receiver and after applying bending corrections

	Above 0°	Above 5°	Above 12°
<i>Sideways</i>			
L1	6/27	7/25	13/27
L2(C)	-1/38	2/37	11/39
L2(P)	-3/67	4/55	19/45
<i>Upright</i>			
L1	6/109	-13/116	-53/131
L2(P)	-55/102	-17/86	-53/145

Mean differences are observed leveling minus nominal leveling

this residual elevation-dependent error is due to deficiencies in the tropospheric bending estimates or due to additional non-tropospheric effects present in the SNR signal, for which the sea state is one of the main candidates (Santamaría-Gómez et al. 2015). On the other hand, the consistency of the leveling values among the different signals between 5 and 25° is a compelling result indicating that L2(P) SNR observables provide similar results as L1 or L2(C). Leveling results from the L2(P) code are, however, more scattered than those from L1 or L2(C), and thus, more SNR series must be integrated to achieve the same precision (Table 1).

Mean leveling differences and scatter from the upright antenna, processed using the new EKF filter methodology, are larger than for the sideways antenna, especially above 12° elevation where very few and scattered frequency estimates were retained after the EKF fit. We also note that while the EKF results in L2(P) are similar to those published in Santamaría-Gómez et al. (2015), the results in L1 do not reproduce the leveling bias of 12 cm. They used SNR data in logarithmic scale with an equivalent noise bandwidth of 1 Hz, different to the optimized bandwidth of 7 Hz and linear SNR data that we used here. We observed that when using logarithmic SNR data within the EKF approach at this site, the leveling bias in L1 rises from 6 mm to 10 cm. Therefore, we explain the leveling bias reported at this site from a combination of very low-elevation data and a non-optimized sinusoidal oscillation in the logarithmic SNR data.

The lower spectral resolution of the SNR data from the upright antenna may also affect the accuracy and precision of the leveling results at this site. The spectral resolution is important because it is a measure of the minimum vertical separation that can be discriminated in the SNR oscillation between two different reflectors. For example, in the spectral domain, a SNR oscillation on the L1 carrier between 2 and 8° elevation from the upright antenna, corresponding to the pink line in Fig. 3, cannot discriminate between two reflectors separated vertically by about 1 m. If there were another reflector within 1 m of the sea surface, the peak in the spectrum of this particular recorded SNR oscillation will account for both reflectors and the estimated distance to the sea surface will be less precise. In contrast, the longer series of SNR oscillations from the antenna orientated sideways provides improved spectral resolution and thus better isolation of the sea-surface reflections in those situations where the sea surface is close to other potential reflectors. This limitation of the technique does not apply in sites where the mean sea level is far from other height-fixed reflectors, for instance the ground or support structures around the antenna, or where the tidal range is large enough to discriminate the sea surface from other reflectors when

correcting the SNR observations with the inverse Doppler-like SSH (Santamaría-Gómez et al. 2015). At the Spring Bay site, the tidal range varies between 0.5 and 1.3 m, and, therefore, it does not provide a significant discrimination with respect to its SNR spectral resolution. However, the height-fixed reflectors are likely far enough to the mean sea surface which is about 3 m below at this site (Fig. 2).

The mean leveling differences for the upright antenna also contain errors in the phase center calibration of the GNSS antenna which, for the upright configuration, are expected to be larger in the vertical direction and thus having more impact on the results than those obtained from the sideways antenna. Errors in the antenna phase center show up in the leveling differences, but they must be considered as a limitation of the classical leveling approach and not as a limitation of this technique, which is insensitive to this error. In this regard, since the effects affecting the frequency of the SNR oscillation, e.g., refraction or sea-surface flatness, are mostly common to the sideways and upright antennas, the differences in the SNR frequency from simultaneous observations and two differently oriented antennas will reflect the height difference between their respective antenna phase centers. Assuming that the relative error of the antenna phase center is one order of magnitude smaller than its value, this technique could be used as an alternative and relatively simple in situ and site-specific validation method for the vertical phase center of the upright antenna that accounts for near-field multipath.

The mean and standard deviation of the leveling differences may also include the contribution of a TG calibration error and TG measurement noise at the millimeter level. Using the radar TG instead of the acoustic, we found mean leveling differences of about 7–8 mm in agreement with the closure error between both TGs. We attribute this leveling difference to the unknown calibration of the radar TG zero. With respect to any time-variable measurement bias at the acoustic TG, the scatter of the leveling results was too large to allow identifying this as a source of error. However, the mean leveling differences obtained using a month of data indicates that this technique could be useful to constrain mean calibration bias and to monitor bias drift of the TG zero at the millimeter level.

Conclusions

We have improved the GNSS reflectometry tie technique for remote TG leveling. We optimized the unknown receiver bandwidth to convert the observed carrier-to-noise density ratio (C/N_0) into linear SNR values and then we developed the processing of the SNR series through an extended Kalman filter/smoothing algorithm. This new

approach allowed us to estimate small but significant changes in the frequency of the SNR oscillation by elevation angle.

We tested the new processing approach in a field experiment conducted at the Spring Bay TG, Australia. We demonstrated that changes in the frequency of the SNR oscillation at very low elevation angles are mostly related to the geometric bending of the radio waves traversing the troposphere and that they can be largely corrected using local atmospheric pressure and temperature observations. We also demonstrated that the leveling bias of 12 cm found at this site is not related to the GNSS equipment but originated from a non-optimized sinusoidal SNR oscillation at very low elevation angles.

Using SNR series above 5° elevation from a GNSS antenna placed with the ground plane vertical, but orientated in azimuth facing the sea surface, we obtained leveling differences at the millimeter level with respect to the nominal leveling from in situ classical surveying techniques. When using the common upright antenna configuration, we obtained leveling differences of less than 2 cm. In this case, the leveling differences may include errors in the GNSS antenna phase center calibration, which are avoided with this technique but not in the classical surveying techniques. The increased scatter of the leveling results from the upright antenna requires further understanding and modeling of the SNR observables.

The leveling differences may also account to some extent for errors in the calibration of the TG zero and for systematic phase effects affecting differently the SNR data in the L1, L2(C) and L2(P) signals tested. For instance, a spurious secondary peak was detected in the spectra of the L2(P) SNR series. The origin of this secondary peak remains unanswered, but its consistent location in the spectrum allowed us to remove its effects and to obtain reliable leveling results from the L2(P) signal.

These results demonstrate the usefulness of the GNSS-R technique to obtain precisely and remotely the leveling between a GNSS antenna and a TG, and the methodological improvements provided here could be incorporated in different applications using reflected GNSS signals. This technique can be applied continuously, providing an independent and economical means to monitor the stability of the TG zero. In addition, the technique offers the potential to be used in a campaign style mode to yield the connection between a TG zero and a nearby continuously operating GNSS site that may not necessarily be in view of the sea. In this case, a mount is required that permits the campaign-based antenna to be orientated sideways, and then reverted to the nominal orientation, enabling data collection for both GNSS-R and a short baseline connection with the existing GNSS site. In addition to the leveling of tide gauges, several applications using reflected GNSS

signals, such as extracting soil moisture, vegetation index or snow depth, could benefit from the simple correction of the tropospheric bending effect at elevation angles below 10° .

Acknowledgments A.S.G. is a recipient of a FP7 Marie Curie International Outgoing Fellowship (Project Number 330103). We acknowledge Geoscience Australia for providing the three GNSS receivers and the GPS data at Spring Bay, and Lachlan Nicholls (Bureau of Meteorology, Australia) for providing and discussing the tide gauge and meteorological data. We acknowledge comments provided by M.A. King, Kristine M Larson and an anonymous reviewer provided comments that helped to improve the manuscript. Google Earth provided the satellite image of Fig. 1.

References

- Anderson KD (2000) Determination of water level and tides using interferometric observations of GPS signals. *J Atmos Oceanic Technol* 17:1118–1127. doi:[10.1175/1520-0426\(2000\)017<1118:DOWLAT>2.0.CO;2](https://doi.org/10.1175/1520-0426(2000)017<1118:DOWLAT>2.0.CO;2)
- Bennett GG (1982) The calculation of astronomical refraction in marine navigation. *J Navig* 35:255–259. doi:[10.1017/S0373463300022037](https://doi.org/10.1017/S0373463300022037)
- Benton CJ, Mitchell CN (2011) Isolating the multipath component in GNSS signal-to-noise data and locating reflecting objects. *Radio Science* 46:n/a-n/a doi:[10.1029/2011RS004767](https://doi.org/10.1029/2011RS004767)
- Dee DP et al (2011) The ERA-Interim reanalysis: configuration and performance of the data assimilation system. *Q J R Meteorol Soc* 137:553–597. doi:[10.1002/qj.828](https://doi.org/10.1002/qj.828)
- Hunter JR (2003) On the temperature correction of the aquatrak acoustic tide gauge. *J Atmos Oceanic Technol* 20:1230–1235. doi:[10.1175/1520-0426\(2003\)020<1230:OTTCOT>2.0.CO;2](https://doi.org/10.1175/1520-0426(2003)020<1230:OTTCOT>2.0.CO;2)
- Jazwinski AH (1966) Filtering for nonlinear dynamical systems. *Autom Control IEEE Trans* 11:765–766
- Larson KM, Nievinski FG (2013) GPS snow sensing: results from the EarthScope plate boundary observatory. *GPS Solut* 17:41–52. doi:[10.1007/s10291-012-0259-7](https://doi.org/10.1007/s10291-012-0259-7)
- Larson KM, Löfgren JS, Haas R (2013a) Coastal sea level measurements using a single geodetic GPS receiver. *Adv Space Res* 51:1301–1310. doi:[10.1016/j.asr.2012.04.017](https://doi.org/10.1016/j.asr.2012.04.017)
- Larson KM, Ray RD, Nievinski FG, Freymueller JT (2013b) The accidental tide gauge: a gps reflection case study from Kachemak Bay, Alaska. *Geosci Rem Sens Lett IEEE* 10:1200–1204. doi:[10.1109/LGRS.2012.2236075](https://doi.org/10.1109/LGRS.2012.2236075)
- Löfgren JS, Haas R, Scherneck H-G (2014) Sea level time series and ocean tide analysis from multipath signals at five GPS sites in different parts of the world. *J Geodyn* 80:66–80. doi:[10.1016/j.jog.2014.02.012](https://doi.org/10.1016/j.jog.2014.02.012)
- Nievinski FG, Larson KM (2014) Inverse modeling of GPS multipath for snow depth estimation—part I: formulation and simulations. *Geosci Rem Sens IEEE Trans* 52:6555–6563. doi:[10.1109/TGRS.2013.2297681](https://doi.org/10.1109/TGRS.2013.2297681)
- Roussel N, Frappart F, Ramillien G, Desjardins C, Gegout P, Pérosanz F, Biancale R (2014) Simulations of direct and reflected waves trajectories for in situ GNSS-R experiments. *Geosci Model Dev Discuss* 7:1001–1062. doi:[10.5194/gmdd-7-1001-2014](https://doi.org/10.5194/gmdd-7-1001-2014)
- Santamaría-Gómez A, Watson C, Gravelle M, King M, Wöppelmann G (2015) Levelling co-located GNSS and tide gauge stations using GNSS reflectometry. *J Geod* 89:241–258. doi:[10.1007/s00190-014-0784-y](https://doi.org/10.1007/s00190-014-0784-y)
- Scargle JD (1982) Studies in astronomical time series analysis. II—statistical aspects of spectral analysis of unevenly spaced data. *Astrophys J*. doi:[10.1086/160554](https://doi.org/10.1086/160554)
- Shih HH, Rogers D (1981) Error analysis for tide measurement systems utilizing stilling wells. NOAA Tech Rep, US Department of Commerce, NOAA, Office of Ocean Technology and Engineering Services



Alvaro Santamaría-Gómez received his Ph.D. in geodesy from the Astronomy and Astrophysics Doctoral School of Paris, France, in 2010. He is an EU Marie Curie Research Fellow with University of La Rochelle, France, and University of Tasmania, Australia, where he works in the field of the earth surface deformation and sea-level change.



Christopher S. Watson received his Ph.D. in geodesy from the University of Tasmania, Australia, in 2005, where he is now a Senior Lecturer. His research interests are focused on the use of space geodetic techniques such as satellite altimetry and GNSS applied to global climate change, sea-level and earth deformation studies.